IEEE Access
Multidisciplinary | Rapid Review | Open Access Journal

Received 28 October 2022, accepted 8 November 2022, date of publication 21 November 2022,
date of current version 30 November 2022.

Digital Object Identifier 10.1109/ACCESS.2022.3223354

RESEARCH ARTICLE

Method for Identification of Multiple Low-Voltage Signal Sources Transmitted Through a Conductive Medium

SAINA NAMAZIFARD, RICHIE RANAISA DARU, KRISTIN TIGHE, KAMESH SUBBARAO, (Senior Member, IEEE), AND ASHFAQ ADNAN
Mechanical and Aerospace Engineering, University of Texas at Arlington, Arlington, TX 76019, USA

Corresponding authors: Ashfaq Adnan (aadnan@uta.edu) and Kamesh Subbarao (subbarao@uta.edu)

This work was supported by the Office of Naval Research (ONR) under Grant N00014-21-1-2051 and Grant N00014-19-1-2383.

ABSTRACT Accurate detection of oscillatory electrical signals emitted from remote sources is necessary in many applications but poses several challenges. The major challenge is attributed to the source voltage and conductivity of the medium through which signals must transmit before they can be sensed by the receiving electrodes/sensors. This study introduces a novel algorithm to optimize source identification where low-voltage (mV range) signals transmit through a conductive medium. The proposed algorithm uses the measured data from different oscillatory signal sources and solves an inverse problem by minimizing a cost function to estimate all the signal properties, including the locations, frequencies, and phases. To increase the overall signal accuracy for a wide range of initial guess frequencies, we have utilized the Lomb-Scargle spectral analysis along with the Least Squares error optimization method. The data utilized in this study comes from an experimental setup that includes a bucket filled with salt-water as the conductive medium, multiple low-voltage signal sources and 32 remotely located sensors. The sources generate sine waves with amplitude of 10 mV and frequencies between 10 – 40 Hz. The average signal-to-noise ratio is approximately 10 dB. The algorithm has been validated using a single-source and multi-source setup. We observed that our algorithm can identify the source location within 10 mm from the actual source immersed inside the bucket of radius $=\sim$ 90 mm. Moreover, the frequency estimation error is nearly zero, which justifies the effectiveness of our proposed method.

INDEX TERMS Source localization, least squared error, multi-sources, inverse problem.

I. INTRODUCTION

Detecting the specific location of an electrical signal source immersed in a conductive medium is one of the critical problems in signal identification applications. Most prominent applications include underwater source localization [1], [2] and the Electroencephalography(EEG)/ Magnetoencephalography(MEG) signal source localization [3]. The underwater source localization application can vary from underwater vehicle tracking to a vital task like an underwater rescue mission. The EEG/MEG source localization is also important since it is directly related to neurological disorders and can affect human health. It is certain that the application of optimized source localization algorithm is versatile and can be used to solve many critical problems including the ones mentioned. In the mentioned cases, the process starts with an electrical signal source that generates an electrical signal. Then signal transmits through a medium from the source to the sensors. Next, the signal is analyzed. These steps collectively provide the spatial location of the electrical source. Since each application involves different environmental conditions, the source identification algorithm must be adapted to ensure accuracy.

The EEG/MEG source localization process is essential in detecting different neurological diseases. In principle, an EEG is used to detect brain signals [4] and an MEG is

The associate editor coordinating the review of this manuscript and approving it for publication was Shovan Barma.

used to detect the magnetic fields produced by the electrical current inside the brain [5]. In both detection processes, the human head acts as a conductive medium where its outer surface is used for sensors (i.e. electrodes) to sense signals that are generated somewhere beneath the inner surface (i.e. specific brain signals) [6], [7]. In other words, the human head transmits the source generated inside the brain to the electrodes attached to the head. Then recorded data is used for source localization of that electrical signal source. A healthy human brain generates brain waves with a specific range of frequencies and amplitudes [8], [9]. Following some specific motor or sensory activities, the frequencies and amplitudes of the brain waves change. By comparing and analyzing the recorded EEG data, before and after the specific activities, any sign of abnormalities at a particular region of the brain can be predicted [10]. Over the past several years, various methods have been used to solve the localization problem [11]. Note that, there are different applications such as image processing [12], [13], [14], fault location in grounded/ungrounded and high-resistance systems [15], and sound source localization [16], [17]. Depending on the application, the solution methodologies are different. In principle, all these methods solve an inverse problem. Nevertheless, all methods have their own advantages and limitations.

The Minimum Norm (MN) method for this application was first introduced in 1994 [18] to solve the specific inverse problem and source localization from EEG signals. This method is proper for noise-free signal analysis, but it does not provide a good result for the deep source localization cases where noise can be inherently present in the signal source. In the same year, a new algorithm called Low Resolution Electromagnetic Tomography (LORETA) was introduced [19]. The LORETA can be considered as an integrated method that combines the weighted minimum norm (WMN) technique [20] with the Laplacian operation. It resolves the deep source localization problem of the MN method. However, the low spatial resolution can be the main disadvantage of this algorithm.

Implementing the recursive steps in solving the inverse source localization problem has significantly improved the results. FOCal Underdetermined System Solution (FOCUSS) is one of these methods which utilizes the WMN to solve the recursive process. FOCUSS could solve the problem of low-resolution result with the LORETA algorithm properly [21].

The other popular EEG source localization method is the Recursive multiple signal classification (MUSIC) [22]. This method defines the source (dipole) in a 3D grid head model. The algorithm is based on the idea of finding a signal subspace and addressing if it works the best for the forward model.

Often the existing EEG source localization methods are modified or combined to generate new algorithms. Examples include methods such as Exact low resolution brain electromagnetic tomography (eLORETA), standardized low-resolution electromagnetic tomographic analysis (sLORETA), RAP MUSIC, LORETA FOCUSS, etc [11]. The new methods offer applications beyond the traditional EEG source localization algorithms. For instance, the MUSIC method can also be used in the sound source localization, as illustrated in [23].Another application is the acoustic source localization problem. This usually addresses the source localization for the 2D case (both isotropic and anisotropic plates) and the 3D structures. One of the most famous methods is Beamforming which is also utilized in the EEG source localization problems [24]. The advantage of using such methods over traditional EEG source localization methods is the robust behavior of the noisy data with the White Gaussian noise. Also, a few source localization methods depend on knowing the Time of Arrival (TOA) information [25]. In other words, the time a specific signal needs to travel from the source until it reaches the sensor should be available. However, the Beamforming method works appropriately regardless of having the precise Time of Arrival (TOA). Thus, depending on the situation, these methods can not only be for source localization inside human brain but also used for similar kind of application.

The Least-squares method uses the real collected signal and the signal generated by the hypothetical electrical source to identify the electrical source. Finding the global minimum of these two signal differences provides the final answer to the source estimation [26].

As mentioned earlier, MUSIC [27] is one of the common methods in different application areas and is not only limited to the EEG source localization problems. It should be noted that most of the algorithms mentioned earlier can only detect the location of the sources but not the other features such as the simultaneous detection of frequencies, phases, and amplitudes of the multiple active electrical signal sources. More information about the electrical source can be important for many reasons. For instance, in the case of a rescue mission, there might be other active electrical sources in the water. The specific amplitude and phase information can help distinguish the emergency pulse-generating device from the other electrical sources.

In this study, we have proposed an optimized constrained Least Squares based method to detect the location of multiple signal sources immersed in a conductive medium. This algorithm not only locates the source but can also estimate other oscillatory signal features, such as frequency and phase. Without losing any generality, we applied our algorithm for low-voltage source localization. For experimental verification, we have used a low-voltage signal source and evaluated the effectiveness of our algorithm. The signal sources used were in the mV range. A small lab-scale experimental setup has been developed for validation that includes a system for generating electrical signals, a conductive liquid medium for signal transmission and EEG-based electrodes for detecting signals. To verify the algorithm, input data has been collected from the experiment. The remainder of the manuscript is outlined as follows. First, a mathematical model is defined to simulate the signal measurement process in the Method section. Afterward, an algorithm based on the Least

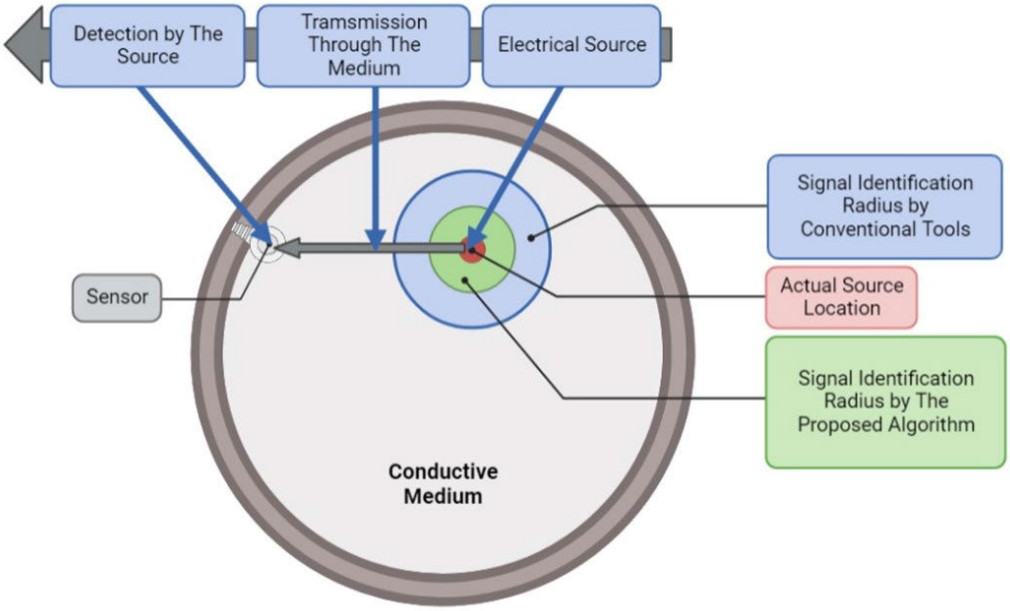

FIGURE 1. Illustration to the general form of the source localization problem.

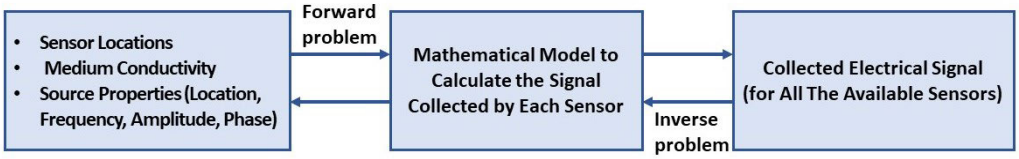

FIGURE 2. Definition of the forward and Inverse problem.

Squares error is introduced to solve the feature identification problem. The Experiment section describes the experimental setup used to generate the data in detail. Finally, the data from the experimental setup is passed to the introduced algorithm to assess its accuracy.

II. METHOD

In a source localization algorithm, it is desired to find a precise estimation of the actual source location. Fig.1 schematically defines the problem. It can be inferred from Fig. 1 that while the exact location of the electrical source is fixed at a point (identified as a red dot), the typical source identification algorithms can only estimate the source location within an area (the green circle). The ideal goal is to reduce the radius of the estimation result (i.e. radius of the green circle) until it gets as small as the red dot. When this happens, it means the source localization method works accurately.

This study aims to introduce an algorithm that not only can precisely detect the source location of an oscillatory signal but also estimate all other characteristic signal features such as the frequency, phase, and amplitude. In general, any source identification problem is solved in two steps. The first step is called the Forward Problem, where the measured signal is simulated mathematically. According to Fig.2, a Forward Problem starts with all the known experimental parameters, such as the location of the sensors, the properties of the electronic signal source (location, frequency, phase, and amplitude), and the medium conductivity. All the mentioned properties are passed to a proper mathematical model that can simulate the signal measured by each sensor. In other words, a forward problem describes the known experimental procedure using mathematical equations.

The second step is the Inverse Problem, which aims to predict the source location. As indicated in Fig.2, this problem starts in the opposite direction to the Forward Problem. In this case, it is assumed that the collected signals from the sensors are available, and by utilizing the present mathematical model, one should be able to find the source location and other features.

A. FORWARD PROBLEM: SOURCE AND SENSORS MATHEMATICAL MODELING

As described earlier, the forward problem begins with determining the source and the sensors model. In our case, we adopted a 2D circular area model with a radius, $R = 88.9\ mm$. It will be discussed later that the radius R in our model reflects the radius of the experimental bucket we used

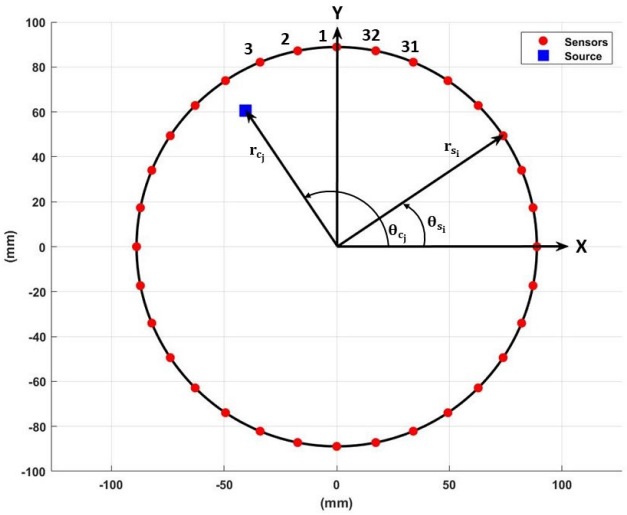

FIGURE 3. 2D model of the sensor and source locations.

for validation. For precise comparison, the exact dimension of the radius is maintained in our model. Figure 3 is a schematic representation of the source and sensors in our 2D space. According to Fig. 3, the locations of the sources and sensors are described by the polar coordinates system. As an example, the location of the i^{th} sensor and j^{th} source are shown as (r_{s_i}, θ_{s_i}) and (r_{c_j}, θ_{c_j}) respectively.

As described later in the experimental setup section, the sensors are located on the circumference of a circle (i.e, the experimental bucket) where the first one is at $(R, \frac{\pi}{2})$. The other sensors are labeled in the CCW direction, as it is shown in Fig. 3. It should be noted that a total number of 32 sensors are considered in our study.

To quantitatively describe the signal generations and detections, one needs to use Maxwell's equations and the Biot-Savart law [28], [29]. In our case, we have combined the two equations, and after some simplification, the expression for describing the measured signal in a 3D half-sphere model is defined as

$$f_{i,j} = \frac{g_j}{4\pi\zeta} \frac{(\boldsymbol{r}_{c_j} - \boldsymbol{r}_{s_i})}{\|\boldsymbol{r}_{c_j} - \boldsymbol{r}_{s_i}\|^3} \boldsymbol{\mu_j} + \boldsymbol{n_i} \tag{1}$$

where $f_{i,j} \in \mathbb{R}^n$ represent the collected signal from the j^{th} source to the i^{th} sensor. Also, in this model, it is assumed that the j^{th} source signal has a specific direction which is identified by a unit vector $\boldsymbol{\mu}_j \in \mathbb{R}^3$ and a magnitude $g_j \in \mathbb{R}$. In order to make the model more realistic, a white Gaussian noise $n_i \in \mathbb{R}^n$ generated from each sensor is added to the model.

This mathematical model however needs to be updated based on the experimental setup and assumptions considered in the present study. Since the source is assumed to generate sinusoidal signals in all directions in the 2D plane while the data samples are recorded. Two significant changes are made to the forward model: 1) The unit vector μ is eliminated and re- placed with a sine wave signal to eliminate the effect of the direction. 2) the vectors $(\mathbf{r}_{c_j} - \mathbf{r}_{s_i})$ are used to calculate the distance between different sources and sensors using the 2-norm as

$$d_{i,j} = \|\boldsymbol{r}_{c_j} - \boldsymbol{r}_{s_i}\| \tag{2}$$

where $d_{i,j} \in \mathbb{R}$ indicates the distance between j^{th} source to the i^{th} sensor.

The above-mentioned changes state that the new mathematical model of the collected signal can be described as shown in Eqn. 3. This model is generated by considering all present parameters in the experiment. The parameters g_j, ζ, ω_j, and ϕ_j are the j^{th} gain, conductivity, j^{th} frequency, and j^{th} phase of the source signal, respectively. Note that these values can be different from each source. Moreover, this model is written in the discrete form to show the collected signals for the k^{th} measured data.

$$f_i(k) = \frac{1}{\zeta} \sum_{j=1}^{P} \frac{g_j}{d_{i,j}^2} sin\left(\omega_j k + \phi_j\right) + \boldsymbol{n_i}, i = 1, \cdots, 32 \tag{3}$$

This equation is the general form for the present study in the presence of P different sources. Eventually, one can put all the collected signals from sensors together to form the general matrix of the measured data for all available N data samples.

$$F = [\boldsymbol{f_1 f_2} \cdots \boldsymbol{f_M}] \tag{4}$$

where $F \in \mathbb{R}^{N \times M}$. Also, in this study $M = 32$.

Now, one can solve the forward problem by knowing the location of the sources and sensors, the magnitude and frequency of the sources, and the conductivity. This is helpful since a well calibrated forward model can be used to predict the expected output.

B. INVERSE PROBLEM: SOURCE LOCALIZATION ALGORITHM

The objective here is to utilize the proposed mathematical model (assumed to be calibrated) to find the location of the source. For this, one should solve an inverse problem where the measured signal Matrix F as in Eqn. 4, the location of the sensors, and the conductivity are available. As mentioned in the introduction section, several different algorithms are available to quantify the source location by solving the inverse problem. This study introduces a new approach based on the Least Squares error. Ultimately, the results from the experimental data illustrate the efficiency of this proposed algorithm.

III. SOLUTION METHODOLOGY: A LEAST SQUARES ERROR BASED SOURCE LOCALIZATION ALGORITHM

This section illustrates the details of the Least Squares error source localization algorithm (LSSL). The idea of implementing this algorithm comes from the EEG source localization problem, which is addressed in [30]. All steps of the LSSL algorithm are briefly shown in a flowchart form in the Fig.4.

In this study, there are a total of five unknowns $(r, \theta, \omega, \phi, g)$ for each source. We estimate these unknown

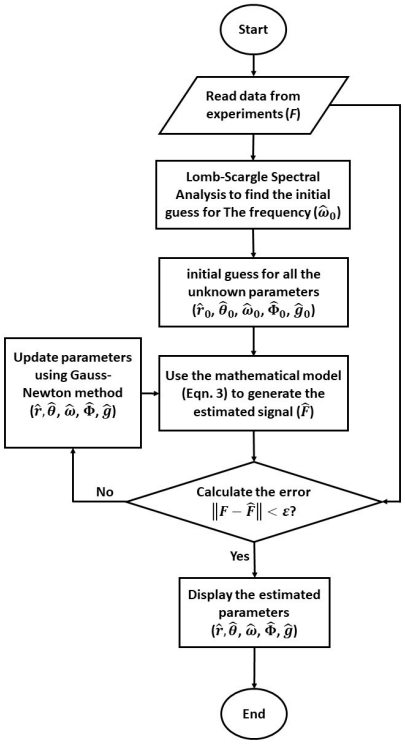

FIGURE 4. **Inverse problem solution using LSSL algorithm illustrated by a flowchart.**

parameters while the estimation problem is optimized and leads to the least estimation error possible.

As it is illustrated in Fig. 4, the estimation process is started with the data from the experiment. The experiment setup is described thoroughly in the following sections. After reading the experimental data, one of the most crucial steps is to determine an initial guess for the frequency of the generated signal from the sources. As outlined in Eqn. 3, the frequency appears in the nonlinear term that makes the estimation process very sensitive to its initial value. Moreover, missing data points while recording the experimental data samples sometimes can occur. Thus, the initial guess process should be robust to an uneven sampling rate. Considering all the mentioned factors to estimate the source frequencies, the Lomb-Scargle Spectral Analysis is the proper method in this study. This method is described by details in [31], where the periodogram for N number of samples is presented in Eqn. 5. In this equation, μ, σ, and τ represent the mean, standard deviation, and time shift, respectively.

$$\boldsymbol{P}(\boldsymbol{\omega}) = \frac{1}{2\sigma^2}\left\{\frac{(\sum_n (x_n-\mu)cos(\omega(t_n-\tau)))^2}{\sum_n cos^2(\omega(t_n-\tau))} + \frac{(\sum_n (x_n-\mu)sin(\omega(t_n-\tau)))^2}{\sum_n sin^2(\omega(t_n-\tau))}\right\}$$

Following the Lomb Scargle Spectral Analysis, a guessed value of $\hat{\omega}_0$ for each source is obtained. It is assumed that each source generates a sine-wave with one particular frequency. However, this method can identify multiple frequency components in a signal, which helps identify multiple frequency components in signal. The next step of estimation is using all five initial guesses ($\hat{r}_0, \hat{\theta}_0, \hat{\omega}_0, \hat{\phi}_0, \hat{g}_0$) to substitute them in the forward model (Eqn. 3) and generate the first estimated signal matrix $\hat{F}$. This synthetic signal is based on the assumed features, and it does not necessarily contain the features present in collected signals. To quantify the difference of the estimated signal and the actual data from the experiment, a cost function is defined. The cost function J is based on the measurement residuals of all 32 available sensors in this study. Now, denoting the decision vector $\hat{\mathbf{x}} = \left[\hat{r}_1\ \hat{\theta}_1\ \hat{\omega}_1\ \hat{\phi}_1\ \hat{g}_1\ \cdots\ \hat{r}_P\ \hat{\theta}_P\ \hat{\omega}_P\ \hat{\phi}_P\ \hat{g}_P\right]^T$, the goal is to minimize the L_2 norm of the cost function, which is defined as

$$J(\hat{\mathbf{x}}) = \left\|F - \hat{F}(\hat{\mathbf{x}})\right\| \tag{5}$$

Note that the estimation result for the radius of the sources cannot be any number larger than the bucket's radius $R = 88.9\ mm$. Thus the optimization of the cost J is subject to the M inequality constraints, $\left\|\hat{r}_j\right\| - R < 0$, for $j = 1, \ldots, P$. The constrained optimization then proceeds along the typical steps outlined in [32] (Chapter 1, section 1.7) by formulating the constraints augmented cost, and deriving the necessary conditions (Kuhn Tucker conditions).

The constrained optimization problem is solved using MATLAB's FMINCON function, with a function tolerance value set to $\epsilon = 1e-6$. The update to the decision vector between iterations uses the Gauss-Newton method (selected in the FMINCON options). The update steps repeat until the cost function reaches its minimum (set to the function tolerance). Eventually, the converged parameters are taken as the final estimation result for all five unknowns for each of the sources.

IV. EXPERIMENTAL SETUP

The experimental setup includes a plastic bucket, 32 sets of scalp electrodes as sensors, and artificially produced electrical signal sources as shown in Fig. 5a. Figure 5 shows the overall set up of the experiment. In this study, wet electrodes have been used [33]. As a conductive medium between the sensors and the source, we use saline water. It should be noted that the experimental technique is applicable to a broad range of conductive mediums. Without losing generality, we have maintained the conductivity of our saline water based on the data presented in [34] and [35]. Accordingly, appropriate salt concentration [36] was used to prepare the desired conductive medium between the sensor and the source. For record keeping purposes, the 32 electrodes are indexed as $A_1 - A_{32}$. Considering the equidistance method used in positioning the electrodes in the electrode-cap, the 32 electrodes were placed radially equidistant from each other. Note that the bucket radius is 88.9 mm. The angle between the two consecutive electrodes was kept at 11.25 degrees. The position of the electrodes inside the bucket was measured using a protractor

and marked for future analysis. A signal generator is used to produce some analog signals inside the conductive saline water. The analog signals were entitled as the source. The distance from the center of the bucket to the point where the source/signal generator is generating the signal is considered as distance 'r'. We have arbitrarily selected the sensor A_{25} as the reference source, and all other subsequent measurements were based on the position and angle of this sensor. As shown in Fig. 5, A_{25} position coincides with the reference axis 'x' and the sensor A1 is aligned with the reference axis 'y'. As such, the angle for sensor A_{25} is measured as zero degrees. Essentially, A1 and A_{25} are orthogonal to each other. The angle between sensor A_{25} and An in the counterclockwise direction is described by positive angle θ. Here n is the number of any sensors between A_{1-A32}.

The rounded part of the electrode was considered as the head of the electrode, and the side that connects with the analog-to-digital (AD) converter was considered as the tail of the electrode (Fig. 5b). The positioning of the electrodes was such that the head of the electrodes would be touching the bottom of the bucket. The tip of the electrode will be aligned with the angular marked-up lines. Each of the electrodes was attached to the bucket using insulation tape. All the output from these receiving sensors was connected to the AD converter of a complete EEG system. A silver chloride stick was used as a signal generator. Silver chloride (AgCl) stick was connected with the data acquisition system (DAQ) through a wire as shown in Figs. 5c and 6a. To make it function like a conductive wire, the AgCl stick was covered everywhere with insulation tape except at the tip. The stick was also inserted inside a plastic straw for added rigidity and ease in handling as shown in Fig. 5c.

Using PATRIOT RS- 232 digitizer which is a serial port connector with a 38400 baud rate, a stylus, and Locator software, we scanned the positioning of each electrode. The scanned data was recorded and applied for the source localization method we used. The electrodes/ sensors keep sensing the data inside the experimental bucket while turned on. Using Biosemi ActiView810-Beta1 software, those sensed data can be observed and recorded. As needed, the EMSE Data Editor Software was used for converting the collected data into suitable file formats for subsequent analysis. It should be noted that the entire experimental setup, as shown in Fig. 5 and 6, is utilized for both single source and multisource experiment. In other words, the positions of the 32 sensors, the bucket and its medium, tools for sensor scanning as well as software for experimental data collection – all were identical throughout the single source and multisource experiments.

The whole experimental setup was covered with RF blocking cloth to minimize any interruption while recording. The sensors are sensitive to electromagnetic fields, strong jerking, vibration, etc. In particular, the sensors that are located in closer proximity with the AD converted appear to be heavily impacted by the undesirable disturbances. As shown in Fig. 6, the experimental setup placed sensor $A_{16} - A_{19}$ closer to the AD converter. All the wiring from 32 sensors was also passed through the side of sensors $A_{16} - A_{19}$. So keeping the signal sources near that section of the bucket always cause some extra cautions and human errors in recorded data. Considering all factors, benchmark trial experiments were conducted to identify the suitable source position that ensures reproducible experiment. It was observed that source located as far as far possible from the AD converter is most suitable for the experiment. For this study, it means the source positioned between A_9 to A_{15} and A_{20} to A_{23} is the best position to use.

A. SOURCE GENERATION

For the experiments, a simple sine wave was used as oscillatory signal source. The 781442-01 | NI USB-6361, X series multifunctional I/O DAQ module (16 AI, 24 DIO, 2 AO) from National Instrument was used for signal generation. Using LabView the system allows pulse width modulation, encoding and frequency measurements and many other functions. The amplitude and frequency were chosen randomly but kept constant for a similar category of experiments. For the single source experiments, a sine wave of frequency 10Hz and amplitude 10 mV was generated. We used two signal sources for multi-source experiments, and two different configurations were also used. Specifically, in the first set of experiments (referred as category 'a'), same amplitude and frequency for both sources are used. For second set (category 'b') different frequencies but same amplitude for each source is used. For category 'a', a set of 10Hz-10Hz frequencies was used. Category 'b' frequency pairs were 31 Hz-10 Hz, 10Hz-31Hz, 40-10Hz, and 10-40Hz. The selection of frequency pairs was random. The tips of the electrodes used as receiving sensors are also made of silver chloride. Using any other material as a source generator creates a change of conductivity in the medium. This affects the homogenous nature of the medium. So the source/ signal generator we used was also made of AgCl. Each source is controlled independently. Table 1 shows the summary of experimental variables.

1) SINGLE SOURCE

For four sensors, $A_9 - A_{12}$, a total of 220 experiments have been conducted. Our experiments have been done for four different conductive mediums. The conductivities of the medium chosen were 2 mS/cm, 4.35 mS/cm, 15 mS/cm, and 20 mS/cm. The values are selected based on [34] and [35]. The single source/signal generator's distances were chosen randomly. The distance was marked and measured before the bucket was filled with the saline water. For convenience, the signal generator was always placed along the radial path of each sensor, as shown in Fig. 5a. For each source position shown in table 2, experiments were done in four of the different conductive mediums. Following each experiment, the source position coordinates, source amplitude and frequency, the conductivity of the medium, and sensor data were recorded. These recorded data are used for validation of our mathematical model.

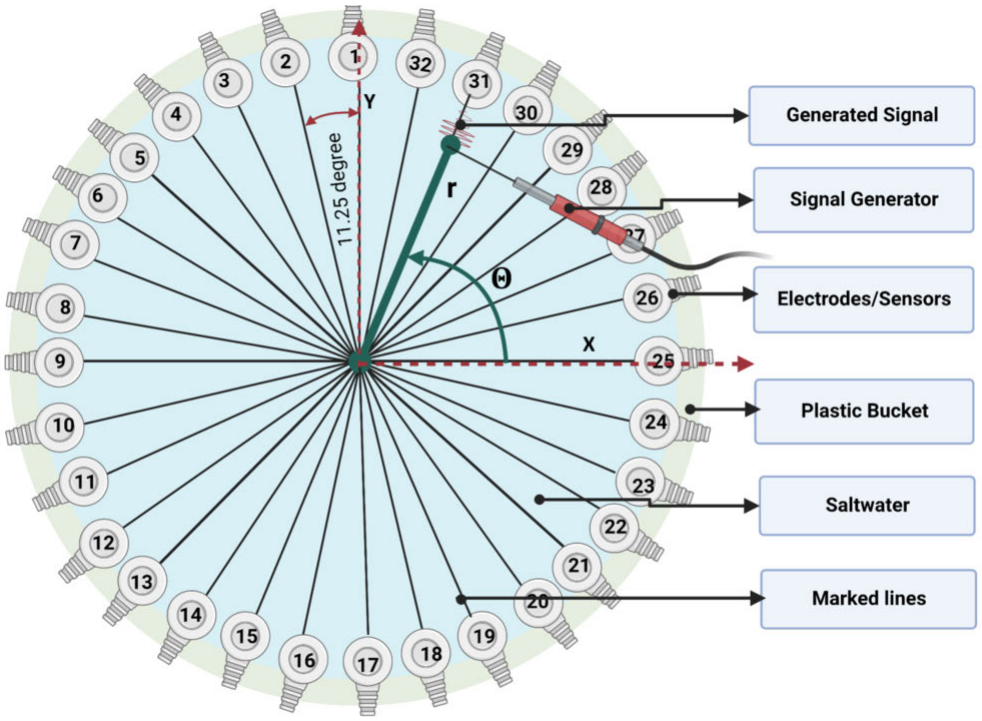

(a)

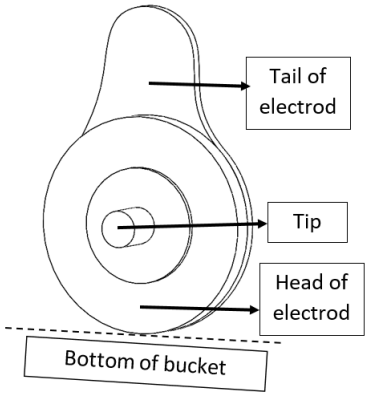

(b)

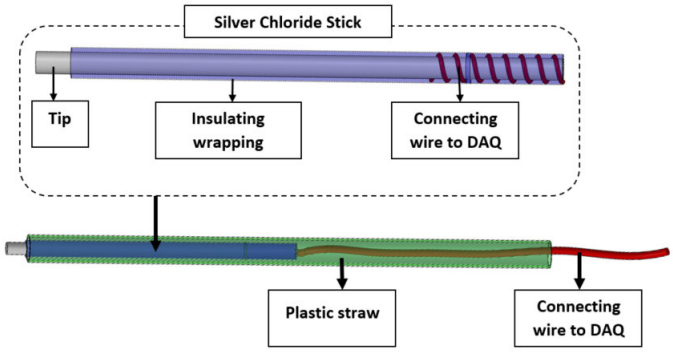

(c)

FIGURE 5. (a) Top view of the experimental bucket of radius R = 88.9 mm showing the 32 sensors, saline water as conductive medium and the artificially generated signal source. (b) Detail view of each electrode/sensor. The electrodes/ sensors are divided into two parts. The Head part of all the sensors makes contact with the bucket. The tail of the electrode is used to attach the electrodes to the surface of the bucket. This tail part also contains wires that connect the electrodes with the AD converter. (c) Detail view of the signal generator.

2) MULTIPLE SOURCES

As outlined in Table 2, seven pairs of electrode positions were selected – three of which are for category 'a' and the rest are for category 'b'. For this, a total of 30 experiments for category 'a' and 40 experiments for category 'b' were conducted. The conductivity for the medium was kept constant at 4.35 mS/cm for category 'a' and 15.2 mS/cm for category 'b'. The distance and the angular position of the sources for both of the categories are shown in table 2.

V. RESULTS AND DISCUSSION

The validation experiments for source identification simulation includes three steps – signal source generation, processing and analysis. Parallelly, the simulation steps are divided into two parts. The first part is called coarse localization. This is also known as visual analysis. The second part is point localization. This step quantitatively determines the near exact location of the source(s) with minimum error.

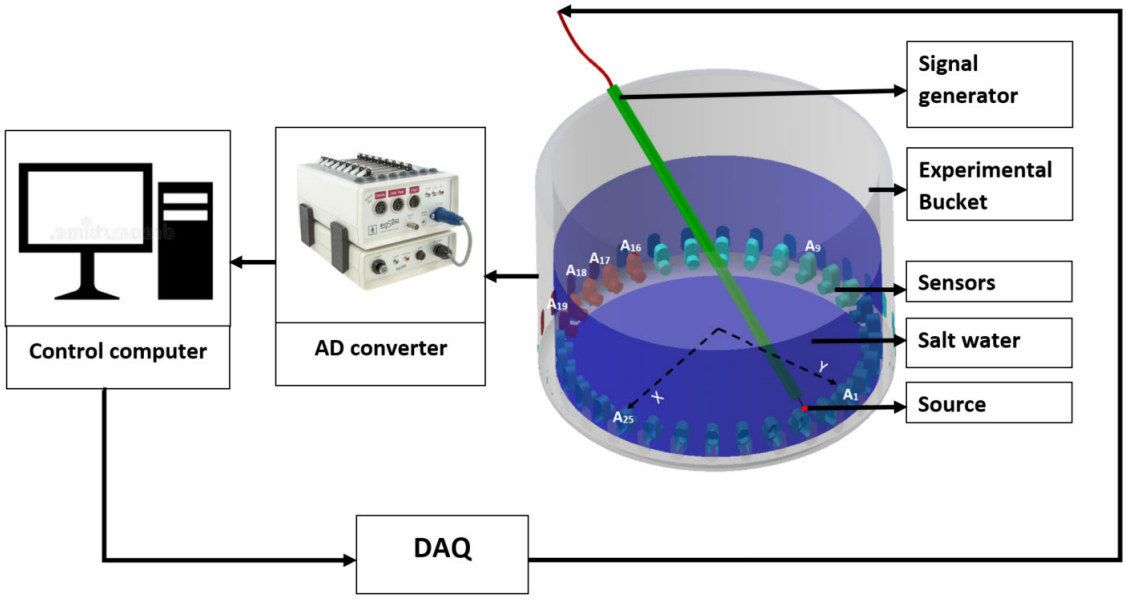

(a)

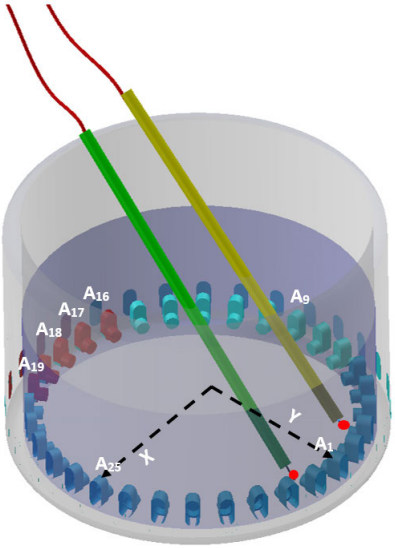

(b)

FIGURE 6. **(a)Experimental setup. The experimental bucket is connected with an AD converter through 32 sensors. The AD converter helps to record real-time data on the computer. The computer is also the controller for the source supply. The amplitude and frequency details are maintained as shown in Table 1. The amplitude and frequencies are controlled through DAQ. For a single source experiment, only one signal generator remains active. For the multi-source experiment, both sources are active. (b) Experimental bucket with two signal generators for multisource experiments.**

A. COARSE LOCALIZATION

We considered the A_{25} position as 0 degrees or the reference. The angle was measured in the counter-clockwise direction. So, the angular position of the 'A_n' sensor will be

$$[(n-1) \times 11.25] + 90 \tag{6}$$

Here n is the number of the sensor that shows the highest signal strength in visual analysis. The simulation result for a single source is shown in Fig. 7a and 7b. It should be mentioned that, the source was kept at $r = 73mm$ and $\theta = 213.75$ degree near sensor A_{12} and the conductivity of the medium was 4.35 mS/cm. It is evident from Fig. 7b that the amplitudes of the signals picked up by the sensors are greatly dependent on the distance between the sensor and the source. It can be observed from Fig. 7b that the signal strength of sensor A_{11} *or* A_{12} is the highest as it is located closest from the signal source. The signal intensities gradually reduce on the adjacent sensors as the distances between the source

TABLE 1. Summary of Sensors, signal amplitude, and frequencies used in the experiment.

Experiment type	Sensors used		Signal amplitude (mV)		Signal frequency (Hz)	
Single source	A_9		10		10	
	A_{10}		10		10	
	A_{11}		10		10	
	A_{12}		10		10	
Multiple sources	Sensors pairs		Signal amplitude (mV)		Signal frequency (Hz)	
Category 'a'	A_9	A_{23}	10	10	10	10
	A_9	A_{10}	10	10	10	10
	A_9	A_{13}	10	10	10	10
Category 'b'	A_9	A_{13}	10	10	31	10
	A_9	A_{13}	10	10	40	10
	A_9	A_{23}	10	10	10	31
	A_9	A_{23}	10	10	10	40

TABLE 2. Source positioning.

Experiment Type	Positioning of the signal generator closer to sensors		r (mm)		$\theta(deg)$	
Single Source	A_9		70		180	
	A_{10}		70		191.25	
	A_{11}		77		202.5	
	A_{12}		73		213.75	
Multiple sources category 'a'	Source 1	Source 2	$r_1(mm)$	$r_2(mm)$	θ_1	θ_2
	A_9	A_{23}	70	73	180	337.5
	A_9	A10	70	70	180	191.25
	A_9	A_{13}	70	73	180	225
Multiple sources category 'b'	A_9	A_{13}	70	73	180	225
	A_9	A_{13}	70	73	180	225
	A_9	A_{23}	70	73	180	337.5
	A_9	A_{23}	70	73	180	337.5

and the sensors increase. Using Eqn. 6, it can be found that the source must be located between $\theta = [202.5, 213.75]$ degrees near sensor $A_{11} or A_{12}$. However, this technique is unable to specify the radial position of the source. As such, the estimation of source location is not a point but a covered area, as shown in Fig. 7a and 7b. The ''out-of-range'' area shown in the Figs. 7a and 7b refers to the region where a presence of source within the area is not reliably detectable by the sensor. For our case, the radius of this ''out-of-range'' circle is about 50 mm.

For multiple source cases, two different source locations are considered. In the first case, as shown in Figs. 7d, the coarse identification process locates the positions of the sources near sensors $A_9 - A_{13}$ and $A_{12} - A_{21}$, respectively. Similarly, for the second case, as shown in Fig. 7f, the positions of the two sources are within the areas covered near $A_9 - A_{13}$ and $A_9 - A_{23}$, respectively. It can be inferred from Figs. 7d, and 7f that, like the single source case, the highest amplitudes recorded by the sensors are near the position of the source. As the distance between the sensor and the source increases, the amplitude of the signal drops. Such trend in signal amplitude variation is also clearly visible when multiple sources are present. As such, the coarse localization method provides a clear indication that the source is located somewhere within the localized region. However, there is a limitation in the coarse localization method. The method is suitable for sources that are located relatively far from each other.

TABLE 3. Simulation result for Single-Source case.

Source #1				
	Initial Guess	Estimation Result	True Value	Error %
r (mm)	85	72.33	73	0.92
theta (deg)	133.75	121.02	123.75	2.21
frequency (Hz)	10.001	10.75	10	7.4952
phase (rad)	0.28	-1.72	N/A	N/A

In such cases, the two sources only weakly interact with other. As a result, the signal strengths in the adjacent sensors are only affected by the nearest source. This is evident in Fig. 7f. When sources are close to each other, then the sources interact strongly with each other. Therefore, the signal strengths in the adjacent sensors are affected by the signals from both sensors. As a result, the coarse method fails to identify the approximate areas of any of the sources, as evident from Fig. 7d. To determine the specific location of the source or sources, regardless the sources are strongly or weakly interacting, a finer identification technique is required. This is the basis for our mathematical model based on the LSSL method. The results are discussed in the following section.

B. IDENTIFICATION USING LSSL METHOD

Now that the experimental data is available, the accuracy of the proposed algorithm can be determined. As mentioned in the previous section, three general cases are considered in these experiments, including 1) single source, 2) strongly

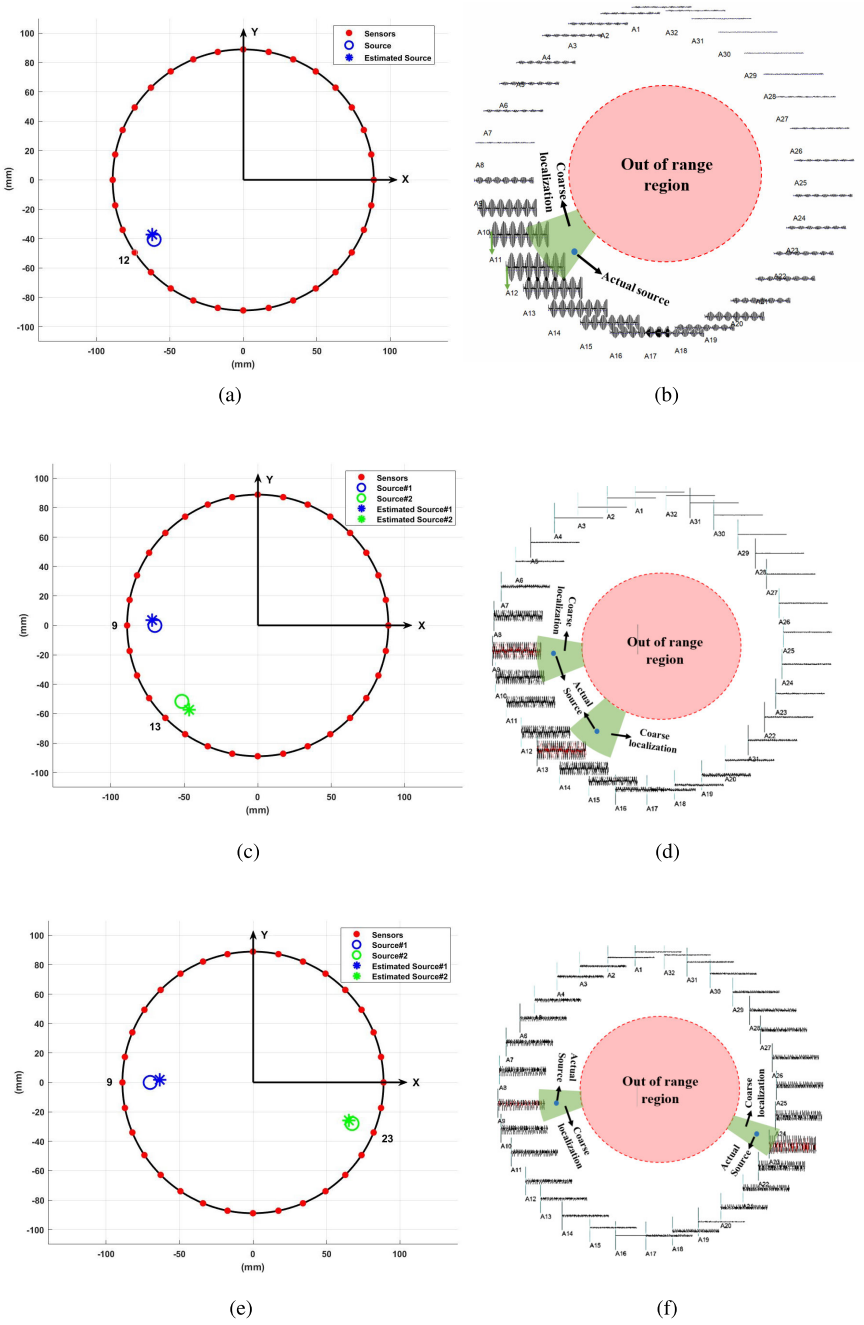

FIGURE 7. Effectiveness of the source identification model for (a), (b) single source near sensor A_{12}. (c), (d) multi-sources near the sensor A_9 and sensor A_{13} and (e), (f) multi-sources near the sensor A_9 and sensor A_3. Note that the actual data point is marked by open circles and estimation is marked by the symbol '*'. Also note the sources in (d) represent strongly interacting sources whereas the sources in (f) represent weakly interacting sources.

interacting multiple sources and 3) weakly interacting multiple sources. Fig.7 represent the source localization results for these three cases.

While Fig.7 is only a representation of the source localization, Tables 3, and 4 provide more details regarding the estimation result of unknown parameters for Single-source and Multi-Sources case, respectively. This table illustrates the details in Figs.7a1, 7b1 and 7c1. In this table, it is important to note that the initial guess for the frequency is significantly close to the real value. This confirms the effectiveness of the Lomb-Scargle method in frequency estimation. To demonstrate the implementation of the Lomb-Scargle algorithm, Fig.8 is also provided. Moreover, to clarify the accuracy of the phase and gain estimation, Fig.9 is provided. This figure

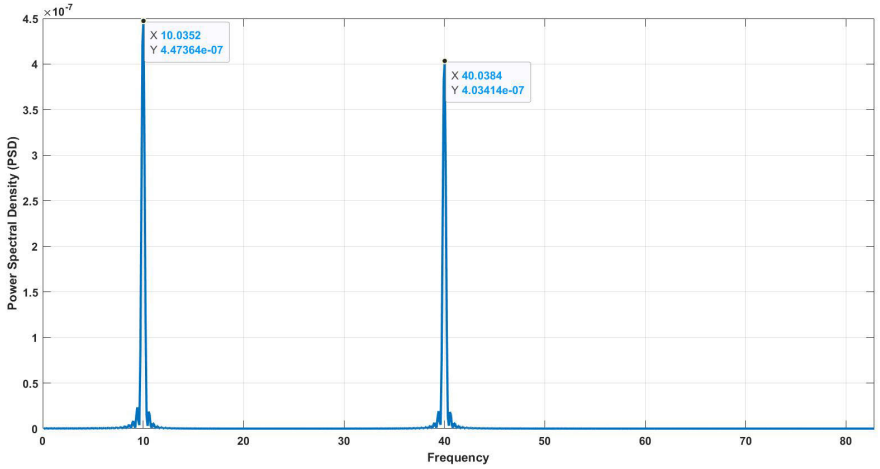

FIGURE 8. Lomb-Scargle Power Spectral Density for two sources with different frequencies.

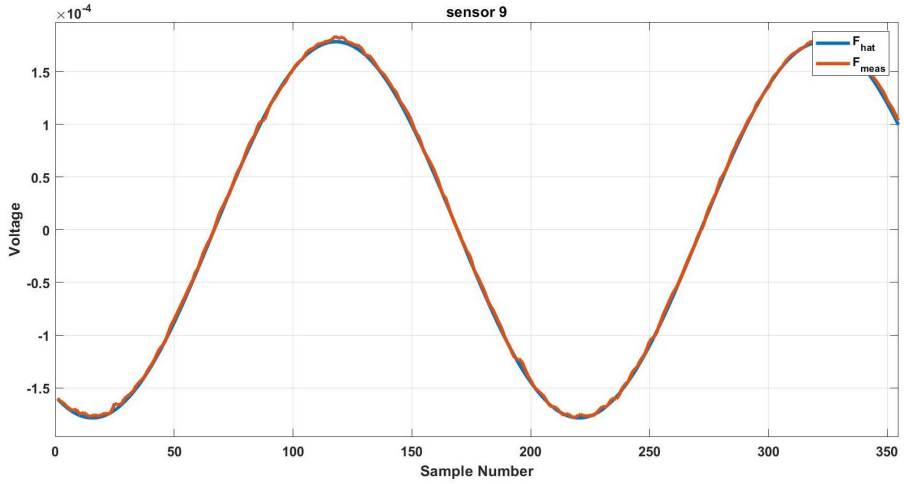

FIGURE 9. Comparing the measured signal (F_{meas}) and the estimated signal result (F_{hat}).

TABLE 4. Simulation result for multi-source case.

	Source #1			
	Initial Guess	Estimation Result	True Value	Error %
r (mm)	75	63.47	70	9.33
$\theta(deg)$	182	178	180	4.81
frequency (Hz)	40.04	40	40	0.00
phase (rad)	-1	-3.01	N/A	N/A
	Source #2			
r (mm)	75	68.69	73	5.90
$\theta(deg)$	330	338.46	337.5	7.20
frequency (Hz)	10.03	9.99	10	0.04
phase (rad)	-0.5	0.18	N/A	N/A

shows the estimated signal in blue and the measured signal in red. Note that these two signals completely cover each other, and the only difference is the noise in the measured data.

Comparing the provided results in the mentioned figures and table illustrate that by increasing the number of sources, the error of the estimation result increases as well. Two main reasons describe this observation. First, by increasing the number of sources, the number of electronic parts increases, leading to more significant noise. Secondly, having more than one source means the unknown variables increase while the amount of the collected signals and the number of sensors remain the same. This means the measured data might not be enough to estimate all the unknowns for a large number of sources.

VI. SUMMARY AND CONCLUSION

In this paper, the problem of source localization is addressed in detail. The solution is solving the inverse problem where the data is available, and the source is unknown. We choose the Least Square Error-based algorithm among all the proposed methods to solve this problem and locate the source of signals. This algorithm is unique as it is not limited to only estimating the location of the source. It is shown that other parameters of the source, such as the frequency and the phase, can be determined using the present algorithm.

As described in this paper, a bucket filled with salt and water is used as an experimental setup. To collect the generated signals, 32 sensors are located inside the bucket. The signal is generated in the sinusoidal form with a specific frequency and location. After collecting the signals, they are used in the LSSL algorithm to solve the inverse problem and find the source properties. All the provided figures and the table in this paper state the presented algorithm's accuracy. In terms of the source localization error, the distance between the source and the estimation results is not greater than 1cm. Comparing this promising result with similar studies like [27] implies the added advantage of the LSSL algorithm.

In Conclusion, the Least Square error-based algorithm can be introduced as an efficient way to solve the inverse problem. Not only the estimation error is significantly lower than the other common methods, but other features like frequency can also be estimated along with the source localization. This study paves the way for further study in signal source localization where significantly large number of sources are present and a non-invasive method is essential for source detection. In other words, in applications where only a forward problem is not practical, this inverse problem method can provide a reliable solution.

CONTRIBUTION STATEMENT

Ashfaq Adnan designs the experiment and Kamesh Subbarao designs the computational model. Richie Ranaisa Daru develops the experimental setup and leads the experimental data collection process. Both Richie Ranaisa Daru and Kristin Tighe perform the experiment. Saina Namazifard sets the computational algorithm and performs all computational analysis. All authors contribute to writing and reviewing the manuscript.

ACKNOWLEDGMENT

The authors would like to thank Dr. Timothy Bentley (Deputy, FHP Program).

(Saina Namazifard and Richie Ranaisa Daru are co-first authors.)

REFERENCES

[1] Y. Xu, W. Xue, Y. Li, L. Guo, and W. Shang, "Multiple signal classification algorithm based electric dipole source localization method in an underwater environment," *Symmetry*, vol. 9, no. 10, p. 231, Oct. 2017.

[2] Y. Xu, W. Shang, L. Guo, J. Qi, Y. Li, and W. Xue, "Active electro-location of objects in the underwater environment based on the mixed polarization multiple signal classification algorithm," *Sensors*, vol. 18, no. 2, p. 554, Feb. 2018.

[3] P. Mégevand and M. Seeck, "Electroencephalography, magnetoencephalography and source localization: Their value in epilepsy," *Current Opinion Neurol.*, vol. 31, no. 2, pp. 176–183, 2018.

[4] I. Ullah, M. Hussain, E.-U.-H. Qazi, and H. Aboalsamh, "An automated system for epilepsy detection using EEG brain signals based on deep learning approach," *Expert Syst. Appl.*, vol. 107, pp. 61–71, Oct. 2018.

[5] G. L. Barkley and C. Baumgartner, "MEG and EEG in epilepsy," *J. Clin. Neurophysiol.*, vol. 20, no. 3, pp. 163–178, May 2003.

[6] H. McCann, G. Pisano, and L. Beltrachini, "Variation in reported human head tissue electrical conductivity values," *Brain Topogr.*, vol. 32, no. 5, pp. 825–858, Sep. 2019.

[7] L. Koessler, L. Maillard, A. Benhadid, J.-P. Vignal, M. Braun, and H. Vespignani, "Spatial localization of eeg electrodes," *Neurophysiol. Clinique/Clin. Neurophysiol.*, vol. 37, pp. 97–102, Apr. 2007.

[8] P. A. Abhang, B. W. Gawali, and S. C. Mehrotra, "Technological basics of EEG recording and operation of apparatus," in *Introduction to EEG- and Speech-Based Emotion Recognition*, 1st ed. New York, NY, USA: Academic, Apr. 2016, pp. 19–50.

[9] M. Teplan, "Fundamentals of EEG measurement," *Meas. Sci. Rev.*, vol. 2, no. 2, pp. 1–11, 2002.

[10] U. R. Acharya, H. Fujita, V. K. Sudarshan, S. Bhat, and J. E. Koh, "Application of entropies for automated diagnosis of epilepsy using EEG signals: A review," *Knowl. Based Syst.*, vol. 88, pp. 85–96, Nov. 2015.

[11] M. A. Jatoi, N. Kamel, A. S. Malik, I. Faye, and T. Begum, "A survey of methods used for source localization using EEG signals," *Biomed. Signal Process. Control*, vol. 11, pp. 42–52, May 2014.

[12] T. Wu, W. Li, L. Li, and T. Zeng, "A convex variational approach for image deblurring with multiplicative structured noise," *IEEE Access*, vol. 8, pp. 37790–37807, 2020.

[13] T. Tirer and R. Giryes, "Image restoration by iterative denoising and backward projections," *IEEE Trans. Image Process.*, vol. 28, no. 3, pp. 1220–1234, Mar. 2019.

[14] Y. Tang, M. Wen, and T. Zeng, "Preconditioned three-operator splitting algorithm with applications to image restoration," *J. Sci. Comput.*, vol. 92, no. 3, pp. 1–26, Sep. 2022.

[15] T. Baldwin, F. Renovich, L. F. Saunders, and D. Lubkeman, "Fault locating in ungrounded and high-resistance grounded systems," *IEEE Trans. Ind. Appl.*, vol. 37, no. 4, pp. 1152–1159, Jul. 2001.

[16] X. Ding, H. Liang, A. Jakobsson, X. Tu, and Y. Huang, "High-resolution source localization exploiting the sparsity of the beamforming map," *Signal Process.*, vol. 192, Mar. 2022, Art. no. 108377.

[17] N. Chu, Q. Huang, L. Yu, Y. Ning, and D. Wu, "Rotating acoustic source localization: A power propagation forward model and its high-resolution inverse methods," *Measurement*, vol. 174, Apr. 2021, Art. no. 109006.

[18] M. S. Hämäläinen and R. J. Ilmoniemi, "Interpreting magnetic fields of the brain: Minimum norm estimates," *Med. Biol. Eng. Comput.*, vol. 32, no. 1, pp. 35–42, Jan. 1994.

[19] R. D. Pascual-Marqui, C. M. Michel, and D. Lehmann, "Low resolution electromagnetic tomography: A new method for localizing electrical activity in the brain," *Int. J. Psychophysiol.*, vol. 18, no. 1, pp. 49–65, Oct. 1994.

[20] O. Hauk, "Keep it simple: A case for using classical minimum norm estimation in the analysis of EEG and MEG data," *NeuroImage*, vol. 21, no. 4, pp. 1612–1621, Apr. 2004.

[21] I. F. Gorodnitsky, J. S. George, and B. D. Rao, "Neuromagnetic source imaging with FOCUSS: A recursive weighted minimum norm algorithm," *Electroencephalogr. Clin. Neurophysiol.*, vol. 95, no. 4, pp. 231–251, Oct. 1995.

[22] J. C. Mosher, P. S. Lewis, and R. M. Leahy, "Multiple dipole modeling and localization from spatio–temporal MEG data," *IEEE Trans. Biomed. Eng.*, vol. 39, no. 6, pp. 541–557, Jun. 1992.

[23] J. Wind, E. Tijs, and H.-E. de Bree, "Source localization using acoustic vector sensors: A MUSIC approach," in *Novem2009: Noise and Vibration: Emerging Methods*. Southampton, U.K.: ISVR, 2009, pp. 1–10.

[24] T. Kundu, "Acoustic source localization," *Ultrasonics*, vol. 54, no. 1, pp. 25–38, 2014.

[25] H. C. So, "Source localization: Algorithms and analysis," in *Handbook of Position Location: Theory, Practice, and Advances*, 2011, pp. 25–66, doi: 10.1002/9781118104750.

[26] R. Grech, T. Cassar, J. Muscat, K. P. Camilleri, S. G. Fabri, M. Zervakis, P. Xanthopoulos, V. Sakkalis, and B. Vanrumste, "Review on solving the inverse problem in EEG source analysis," *J. NeuroEng. Rehabil.*, vol. 5, no. 1, pp. 1–33, Dec. 2008.

[27] Y. Xu, L. Guo, W. Shang, and Y. Li, "Underwater electro-location method based on improved matrix adaptation evolution strategy," *IEEE Access*, vol. 6, pp. 39220–39232, 2018.

[28] Y. Wang, "Successive estimation method of locating dipoles based on QR decomposition using EEG arrays," McMaster Univ., Hamilton, ON, Canada, Tech. Rep., 2007. [Online]. Available: http://hdl.handle.net/11375/22455

[29] S. Baillet, J. C. Mosher, and R. M. Leahy, "Electromagnetic brain mapping," *IEEE Signal Process. Mag.*, vol. 18, no. 6, pp. 14–30, Nov. 2001.

[30] S. Namazifard and K. Subbarao, "Multiple dipole source position and orientation estimation using non-invasive EEG signals," *IEEE Access*, to be published. [Online]. Available: https://www.techrxiv.org/articles/preprint/Multiple_Dipole_Source_Position_and_Orientation_Estimation_using_non-invasive_EEG_Signals/21049585

[31] N. R. Lomb, "Least-squares frequency analysis of unequally spaced data," *Astrophys. Space Sci.*, vol. 39, no. 2, pp. 447–462, Feb. 1976.
[32] A. Bryson and Y. Ho, *Applied Optimal Control: Optimization, Estimation, and Control*. Oxfordshire, U.K.: Taylor & Francis, 1975.
[33] M. A. Lopez-Gordo, D. Sanchez-Morillo, and F. P. Valle, "Dry EEG electrodes," *Sensors*, vol. 14, no. 7, pp. 12847–12870, 2014.
[34] C. Ramon, P. Garguilo, E. A. Fridgeirsson, and J. Haueisen, "Changes in scalp potentials and spatial smoothing effects of inclusion of dura layer in human head models for EEG simulations," *Frontiers Neuroeng.*, vol. 7, p. 32, Aug. 2014.
[35] V. Montes-Restrepo, P. van Mierlo, G. Strobbe, S. Staelens, S. Vandenberghe, and H. Hallez, "Influence of skull modeling approaches on EEG source localization," *Brain Topogr.*, vol. 27, no. 1, pp. 95–111, Jan. 2014.
[36] J. Kamcev, R. Sujanani, E.-S. Jang, N. Yan, N. Moe, D. R. Paul, and B. D. Freeman, "Salt concentration dependence of ionic conductivity in ion exchange membranes," *J. Membrane Sci.*, vol. 547, pp. 123–133, Feb. 2018.

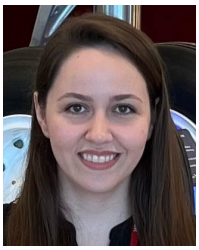

SAINA NAMAZIFARD received the B.Sc. and M.Sc. degrees in mechanical engineering from the K. N. Toosi University of Technology. She is currently pursuing the Ph.D. degree with the Department of Mechanical and Aerospace Engineering, University of Texas at Arlington. She is currently working as a Graduate Research Assistant with the Aerospace System Laboratory (ASL), University of Texas at Arlington (UTA). Her research interests include optimization, biological signal processing, and computational neuroscience.

RICHIE RANAISA DARU received the B.Sc. degree in aeronautical engineering from the Military Institute of Science and Technology, Bangladesh, in 2016. She is currently pursuing the Ph.D. degree with the Department of Mechanical and Aerospace Engineering, University of Texas at Arlington, Arlington, TX, USA. Before starting her Ph.D. degree, she worked as a Lecturer with the Military Institute of Science and Technology, in 2017. Along with her Ph.D. degree, and also currently working as a Graduate Research Assistant with the Multiscale Mechanics and Physics Laboratory (MMPL), UTA. Her current research interests include material development, sensor development and design, and related to smart sensing of brain injury.

KRISTIN TIGHE is currently pursuing the bachelor's degree in mechanical engineering with the University of Texas at Arlington, Arlington, USA. She is an Undergraduate Researcher with the Multiscale Mechanics and Physics Laboratory, UTA. Her research interest includes electrically conductive materials for use in phantom head models.

KAMESH SUBBARAO (Senior Member, IEEE) received the Ph.D. degree from the Department of Aerospace Engineering, Texas A&M University, College Station, in 2001. He is currently a Professor and the Director of the Aerospace Systems Laboratory (ASL), Department of Mechanical and Aerospace Engineering, University of Texas at Arlington (UTA), Arlington, USA. After his Ph.D. degree, he worked as an Applications Developer at the Controls and Systems Identification and Estimation Toolboxes Group, The MathWorks Inc., from 2001 to 2003. He research has been funded by DARPA, NSF, AFRL, ONR, NASA, Lockheed Martin, Whirlpool Inc., Nextgen Aeronautics, and Hypercomp Inc. He received the President's Award for Excellence in Teaching, in 2021, and the Lockheed Martin Aeronautics Company Excellence in Teaching Award, in 2016. He is a fellow of the Royal Aeronautical Society (FRAeS) and the American Astronautical Society. He is also an Associate Fellow of AIAA and Senior Member of ASME.

ASHFAQ ADNAN received the Ph.D. degree in aeronautics and astronautics engineering from Purdue University, in 2008. He is currently a Professor with the Department of Mechanical and Aerospace Engineering, and the Director of the Multiscale Mechanics and Physics Laboratory (MMPL), UTA. Prior to joining UTA in the Fall of 2010, he was a Postdoctoral Research Associate at Northwestern University. His current research interests include cellular level brain injury mechanisms, smart sensing of brain trauma, and additive manufacturing of protective materials. His research funded by multiple Office of Naval Research (ONR) grants and Defense University Research Instrumentation Program (DURIP) grants. He is a member of an interdisciplinary and collaborative research hub called PANTHER that, as a team, investigates the mechanisms, detection, and prevention of TBI. He is an ASME Fellow. He was a recipient of the Department of Navy's inaugural 2021 Distinguished Fellow Program Award. He was also a recipient of the UTA Outstanding Research Award, from 2021 to 2022, and the Lockheed Martin Teaching Award, in 2020.